

CVKAN: Complex-Valued Kolmogorov-Arnold Networks

1st Matthias Wolff
Department of Computer Science
University of Münster
Münster, Germany
matthias.wolff@uni-muenster.de

2nd Florian Eilers
Department of Computer Science
University of Münster
Münster, Germany
florian.eilers@uni-muenster.de

3rd Xiaoyi Jiang
Department of Computer Science
University of Münster
Münster, Germany
xjiang@uni-muenster.de

Abstract—In this work we propose \mathbb{C} KAN, a complex-valued KAN, to join the intrinsic interpretability of KANs and the advantages of Complex-Valued Neural Networks (CVNNs). We show how to transfer a KAN and the necessary associated mechanisms into the complex domain. To confirm that \mathbb{C} KAN meets expectations we conduct experiments on symbolic complex-valued function fitting and physically meaningful formulae as well as on a more realistic dataset from knot theory. Our proposed \mathbb{C} KAN is more stable and performs on par or better than real-valued KANs while requiring less parameters and a shallower network architecture, making it more explainable.

Index Terms—Complex-Valued Neural Networks, Kolmogorov-Arnold Networks, Explainable AI

I. INTRODUCTION

The recently published Kolmogorov-Arnold Network (KAN) [1], [2] has proven to be a successful new approach for problems especially in the field of symbolic function fitting [3] and solving physical equations [4]. Adding to its success is the intrinsic explainability of KANs because of learnable univariate functions on edges instead of linear weights and fixed nonlinear activation functions in classical Multilayer Perceptrons (MLPs). These learned univariate functions hold all model weights and can easily be visualized, thus making it intuitively understandable how single layers impact the model output.

Another emerging field in machine learning research are Complex-Valued Neural Networks (CVNNs), which have shown great success in a multitude of applications as well as good theoretical properties in terms of overfitting and generalization [5], [6]. Especially for applications with complex-valued input types, these models have shown promising results.

In this work we aim to combine the advantages of KANs and CVNNs within our proposed Complex-Valued Kolmogorov-Arnold Network (\mathbb{C} KAN). By replacing the learnable real-valued functions on the edges of a KANs with learnable complex-valued functions we maintain the intrinsic explainability of KANs while also leveraging the direct use of complex-valued functions, making it more fit for problems requiring complex-valued calculations.

The original KANs used fitting of B-Splines to learn the edge functions, however this training is rather slow and can be unstable, thus [7] proposed to replace the originally used B-Splines with easier to learn Radial Basis Functions (RBFs).

While it would be possible to utilize complex-valued B-Splines [8]–[10] to construct a complex-valued KAN, we propose to adopt the idea of RBFs to the complex domain, to benefit from their easier and faster training process. Additionally, we propose to replace the tedious dynamic grid extension used in KANs by Batch Normalization to prevent the model to fall outside the predefined grid.

Overall, our contributions can be summarized as:

- We adopt the KAN framework to the complex domain by utilizing complex-valued RBFs.
- We propose to add a normalization layer to efficiently solve the problem of fixed grid sizes.
- We propose a framework to utilize the explainability of KANs in the complex domain.
- We provide our code, both for training the model and the visualization, as an open source library to promote open science. ¹

We evaluate our approach against real-valued baselines on three datasets and conduct ablation studies on normalization schemes as well as explainability.

II. RELATED WORK

A. KANs

After the recent introduction of KANs by Liu et al. [1], [2] there has been a great variety of attempts to apply the ideas of KANs to different fields like image processing [11], satellite image segmentation [12], graph neural networks [13], [14] and even transformers [15]. Hou et al. [16] give a great overview of the different applications and extensions of KANs. Their explainability can be of great value in fields where machine learning approaches are strongly regulated like survival analysis in medicine or engineering [17]. Multiple works have already benchmarked the performance of KANs against MLPs [3], [18] and found KANs to be a more suitable alternative in some fields. Alter et al. [19] found that large-scale KANs are more robust against adversarial attacks as MLPs and thus form an interesting direction for further research in multiple fields.

In [4] the authors explore different partial differential equation forms based on KAN instead of MLP for solving forward and inverse problems in computational physics. A systematical

¹Link to code base: <https://github.com/M-Wolff/CVKAN>

comparison demonstrates that the KAN approach significantly outperforms MLP regarding accuracy and convergence speed. Further successful applications of KAN can be found for operator learning in computational mechanics [20] and image classification [21].

B. Complex-Valued Neural Networks

After early introduction of CVNNs [22] they have lately risen in popularity since the introduction of building blocks for deep learning architectures [23]. Since then a lot of theoretical contributions have been made [24]–[26] to enable a multitude of applications [27]–[31].

The most closely related prior work in the complex domain are deep complex Radial Basis Function Neural Networks (CRBFNs) [32], [33]. However, in CRBFNs, the RBFs are applied to all inputs of a neuron (e.g. vertex of the computational graph) simultaneously, while in CKANs the RBFs are applied on the edges of the computational graph to each value individually. Thus CRBFNs are architecturally more similar to classical MLPs with RBFs as activations functions, where we aim to adopt the KAN framework to the complex domain.

III. REAL-VALUED KANS

The Kolmogorov-Arnold representation theorem (1) [34] states that any continuous function can be represented by a superposition of univariate functions.

$$f(x_1, \dots, x_n) = \sum_{q=1}^{2n+1} \Phi_q \left(\sum_{p=1}^n \phi_{q,p}(x_p) \right) \quad (1)$$

This formula can be used to construct a two layer neural network with n inputs, one output and learnable functions $\Phi_q, \phi_{q,p}$. For each layer and each feature an individual univariate function has to be learned, so combination of features is only done by summing the outputs of all these functions. While theoretically possible, this theorem was long deemed to be of little use for machine learning [35], because the inner functions can be highly nonsmooth.

However, Liu et al. [1] have generalized this formulation of only one hidden layer of size $2n + 1$ and one single output to arbitrary network depths L and layer widths n_l with $l = 0 \dots L - 1$ to overcome the problem of nonsmooth inner functions. Let $N_{l,i}$ be the i -th neuron in layer l , then every node $N_{l,p}$ in layer l is connected to every node $N_{l+1,q}$ in the following layer by an edge $E_{l,q,p}$ with $p = 1 \dots n_l$ and $q = 1 \dots n_{l+1}$. On every edge there is one learnable univariate function $\phi_{l,q,p}$ and the values of all incoming edges into a single node of the next layer are summed. This way the multiplication with linear weights between layers in classical MLPs has been replaced by learnable univariate functions and the nonlinear but fixed activation functions in the nodes of MLPs have been replaced by plain summation. In the original KAN the functions are learned using B-Splines [1], [2].

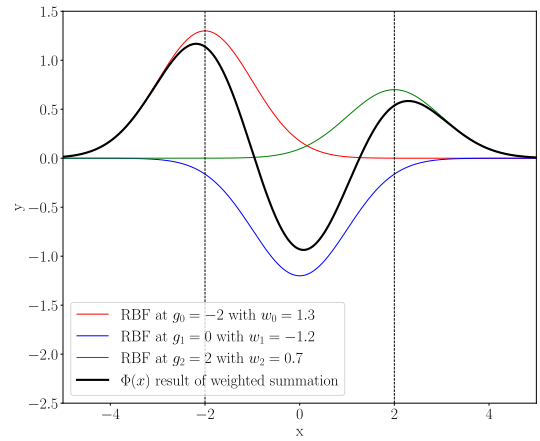


Fig. 1. Visualization of a weighted sum of three RBFs with a grid in the interval $[-2, 2]$ and grid points at $g_0 = -2, g_1 = 0, g_2 = 2$.

A. Real-valued RBFs

The way B-Splines are used to learn the functions in KANs [1], [2] is computationally intensive and slow. Thus different improved methods for learning a function have been proposed like DeepOKAN [20] or FastKAN [7], in which the authors suggest to replace B-Splines with RBFs for faster computation. Equation (2) describes a RBF that is symmetrical and centered around 0.

$$\phi(x) = \exp(-x^2) \quad (2)$$

To represent more complicated functions multiple RBFs are centered around uniformly distributed grid points g_i inside a fixed grid with $i = 0 \dots G - 1$ and G denoting the number of grid points. All those RBFs are then combined in a weighted sum with learnable weights $w_i \in \mathbb{R}$ to construct one continuous function over the whole grid (3).

$$\Phi(x) = \sum_{i=0}^{G-1} (w_i \phi(x - g_i)) \quad (3)$$

The number of grid points G and the range of the grid $[a, b]$, over which the RBFs are defined, are hyperparameters. By making the grid finer one can represent more complicated functions with increasing precision.

IV. COMPLEX-VALUED KANS

To extend KANs into the complex-valued domain we need a way to learn functions $f : \mathbb{C} \rightarrow \mathbb{C}$ on every edge. Inspired by the use of RBFs in FastKAN we propose to construct those complex functions using multiple RBFs on a 2D grid. Furthermore we employ a complex-valued equivalent to the Sigmoid Linear Unit (SiLU) function used in KANs and make use of Batch Normalization to stay inside our fixed range grid. Finally we present a tool for visualizing the CKAN to make it interpretable and explain its inner workings.

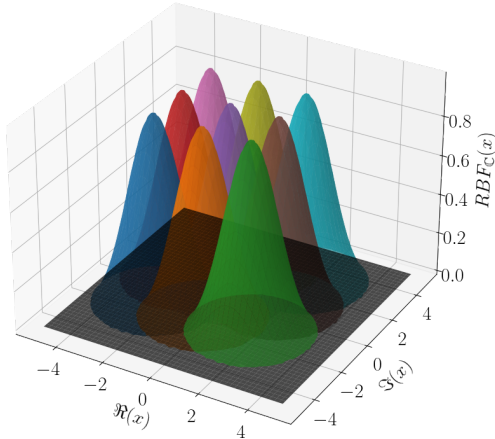


Fig. 2. Visualization of the complex RBFs with a grid in the interval $[(-2 - 2i), (2 + 2i)]$ and $G = 3$ grid points per dimension resulting in $3 \cdot 3 = 9$ grid points.

A. Complex-valued RBFs

Chen et al. [32] have chosen to treat real and imaginary parts separately and construct a complex-valued RBF out of two real-valued RBFs which only depend on the real or imaginary part of the input each. On the other hand Soares et al. [33] use a single real-valued RBF that depends on both the real and imaginary parts of the input jointly. While the latter apply these multivariate RBFs inside vertices, we propose to use univariate RBFs on edges instead to maintain the idea of KANs and achieve higher explainability. We define a RBF $\mathbb{C} \rightarrow \mathbb{R}$ as:

$$\phi_{\mathbb{C}}(x) = \exp(-|x|^2) \quad (4)$$

We can use this RBF in combination with complex-valued grid points and complex-valued weights to learn a complex-valued function. Let $w_{u,v} \in \mathbb{C}$ be learnable weights and $g_{u,v} \in \mathbb{C}$ complex-valued grid points on a grid with $G \times G$ grid points to cover the real and imaginary parts of the input.

$$\Phi_{\mathbb{C}}(x) = \sum_{u=0}^{G-1} \left(\sum_{v=0}^{G-1} w_{u,v} \phi_{\mathbb{C}}(x - g_{u,v}) \right) \quad (5)$$

Note that this calculation is equivalent to learning two functions $\mathbb{C} \rightarrow \mathbb{R}$ separately with twice as many real-valued weights $\Re(w_{u,v}), \Im(w_{u,v}) \in \mathbb{R}$ and treating these as real- and imaginary parts of the functions learned here.

In the special case of a real-valued output (e.g. a classification task), we drop the imaginary part of the weights in the last layer, thus obtaining a function $\mathbb{C} \rightarrow \mathbb{R}$.

In Fig. 2 we depict a visualization of the RBFs on a 2D grid. Each cone at gridpoint $g_{u,v}$, represented by a RBF $\mathbb{C} \rightarrow \mathbb{R}$, gets multiplied by complex-valued learnable weights $w_{u,v}$ to construct a complex-valued output.

B. Residual Activation Function

In the real-valued KANs, a residual activation function is used to help the training of the univariate functions. To this

end an activation function σ is added to the sum of RBFs as explained above. Thus we chose to extend (5) to

$$\Phi_{\mathbb{C}}(x) = \Phi_{\mathbb{C}}(x) + \sigma(x) \quad (6)$$

We propose to use \mathbb{C} SiLU as this residual activation function, a complex-valued equivalent to the SiLU-function (7) used in [1], [2], [7]:

$$\text{SiLU}(x) = x \left(\frac{1}{1 + e^{-x}} \right) \quad (7)$$

$$\mathbb{C}\text{SiLU}(x) = \text{SiLU}(\Re(x)) + i \text{SiLU}(\Im(x)) \quad (8)$$

This residual activation function additionally gets a learning weight and bias, which we also adopt in two ways. First, we use a complex-valued weight $w_{\mathbb{C}} \in \mathbb{C}$ (9) on the output of the full \mathbb{C} SiLU. Second, the real and imaginary parts are each weighted with a real-valued weight $w_1, w_2 \in \mathbb{R}$ separately (10). Both approaches get an additive bias $\beta \in \mathbb{C}$. Thus the two approaches studied in our work are:

$$\mathbb{C}\text{SiLU}_{\mathbb{C}}(x) = w_{\mathbb{C}} (\text{SiLU}(\Re(x)) + i \text{SiLU}(\Im(x))) + \beta \quad (9)$$

$$\mathbb{C}\text{SiLU}_{\mathbb{R}}(x) = w_1 \text{SiLU}(\Re(x)) + i w_2 \text{SiLU}(\Im(x)) + \beta \quad (10)$$

In our experiments in section V we study the difference in performance of both approaches.

C. Complex-valued Batch Normalization

For KANs it is necessary to fix the grid range. However, it is not guaranteed that the output of an intermediate layer (and thus the input of the next layer) stays within a grid that was fixed before training. To tackle this challenge [1] proposed dynamic extension of the grid during training. This is however a time intensive process that might slow down the learning process. Instead we propose to normalize the output of a vertex after summation. We propose to use BatchNorm ($\text{BN}_{\mathbb{R}}$) [36] for the Radial Basis Function based FastKAN [7]. To adapt this to the complex domain, we explore three different complex-valued Batch Normalization approaches.

First, we adapt \mathbb{C} BatchNorm [23], where the covariance matrix of the complex distribution is normalized and an output distribution is learned through a learnable covariance (e.g. a symmetric positive definite) matrix. With \bar{z} , $\text{Cov}(z)$ being the mean and covariance over the batch dimension and $\gamma_{\text{Cov}} \in \mathbb{R}^{2 \times 2}, \beta \in \mathbb{C}$ learnable parameters, it is then defined as:

$$\begin{pmatrix} \Re(\text{BN}_{\mathbb{C}}(z)) \\ \Im(\text{BN}_{\mathbb{C}}(z)) \end{pmatrix} = \gamma_{\text{Cov}} \text{Cov}(z)^{-\frac{1}{2}} \begin{pmatrix} \Re(z - \bar{z}) \\ \Im(z - \bar{z}) \end{pmatrix} + \beta \quad (11)$$

Second, we propose to standardize the variance of the complex-valued input distribution. With \bar{z} , $\mathbb{V}(z)$ being the mean and variance over the batch dimension and $\gamma_{\mathbb{R}} \in \mathbb{R}, \beta \in \mathbb{C}$ learnable parameters, we define it as:

$$\text{BN}_{\mathbb{V}}(z) = \gamma_{\mathbb{C}} \frac{z - \bar{z}}{\sqrt{\mathbb{V}(z)}} + \beta \quad (12)$$

The third approach is to simply normalize the real and imaginary part of the complex-valued inputs separately. This

is equivalent to just applying the real-valued BatchNorm separately to the real and imaginary parts of the input:

$$\text{BN}_{\mathbb{R}^2}(z) = \text{BN}_{\mathbb{R}}(\Re(z)) + i \text{BN}_{\mathbb{R}}(\Im(z)) \quad (13)$$

We employ these three approaches after every but the last layer in our CKAN and study their performance in section V.

D. Interpretability of CVKAN

One major advantage of KANs is their inherent interpretability. Since the KAN learns on the edges, the learned univariate functions are directly applied to each input feature of the current layer. As proposed in [1], [2], we can utilize this property in two ways to explain the inner working of the KAN: We can give importance scores to all edges and vertices to understand which parts of the network significantly influence the output and we can visualize the learned functions on the edges to understand their input-output relation. Both of these can also be utilized for CKANs.

To calculate importance scores for edges and vertices, KAN 2.0 [2] uses the standard deviation of the output of that edge or vertex over the whole dataset distribution to annotate every edge and node with a relevance score by iterating backwards through the network. We adopt this idea and propose to use the standard deviation of the complex distribution. For $z = (z_1, \dots, z_n) \in \mathbb{C}^n$ and \bar{z} its mean, it is defined as:

$$\text{std}(z) = \sqrt{\frac{1}{n-1} \sum_{i=1}^n |z_i - \bar{z}|^2} \quad (14)$$

Fig. 4 presents an example of utilizing the standard deviation to assign relevance scores to edges and vertices as well as visualizing the individual learned edge functions.

For CKAN, the inputs and outputs of edges are complex-valued. To visualize their behavior we thus have to visualize a function $\mathbb{C} \rightarrow \mathbb{C}$. We propose to visualize this as a colored 3D plot, where bases are the real and imaginary part of the input, the height is the magnitude of the output and the color shows the phase of the output. Due to the 2π periodicity of the phase, we choose a periodic color map. In Fig. 3 a small CKAN is visualized as an example.

One limitation to the interpretability in general is the depth of the network. The deeper the network, the harder it is to understand the full model by understanding its subparts. Thus, when evaluating the suitability of a KAN model, the trade-off between model size and performance maximization needs to be accounted for.

V. EXPERIMENTS

To compare our complex-valued CKAN with the real-valued KAN and FastKAN on complex-valued datasets we split the complex numbers of the input and output layer of real-valued KANs into real and imaginary parts. Thus we end up with real-valued KANs that have twice the input and output dimension of our CKAN. We conduct three different experiments.

- Just like in [1], we show that our network is capable of learning simple symbolic correlations between input and

output based on synthetic formulae and outperforms its real-valued opponents on complex-valued problems.

- We extend this synthetic function-fitting task from arbitrary simple functions to more complicated and physically meaningful formulae.
- We use the knot dataset [37], which contains two complex-valued features and was also used by Liu et al. to study the original KAN [1] to analyze the performance of our CKAN on a more realistic dataset and for classification.

For our experiments based on synthetic formulae we sample data points for each variable within our grid range and calculate the target output based on the symbolic formula. Our grid range is always $[-2, 2]$ in \mathbb{R} or $[(-2, -2i), (2, 2i)]$ in \mathbb{C} respectively. Because of Batch Normalization the resulting distribution has a standard deviation of $\sigma = 1$ and mean $\mu = 0$. We use a grid centered around zero spanning two standard deviations in each direction to optimize the trade off between a smaller grid size and minimizing the chance of the output of the former layer exceeding the grid. For the tabular knot dataset [37] we normalize each feature to be inside of our grid. If the dataset contains real-valued features we also feed them into our CKAN as complex-valued numbers but set the imaginary part to zero.

We always apply a 5-fold cross validation. As metrics to evaluate the performance of the models we use Mean Average Error (MAE) and Mean Square Error (MSE) for regression and Cross-entropy (CE)-Loss and Accuracy for classification tasks.

A. Function Fitting

We chose four simple functions with one or two complex-valued input variables (cf. Table I) to demonstrate that our CKAN is capable of learning basic correlations.

For each function from Table I one can determine the required model size by looking at the hierarchy of the function evaluation. Since we can learn any univariate function on a single edge, for f_1 a 1×1 CKAN is optimal in theory. In the real-valued domain we need at least a $2 \times 3 \times 2$ KAN to represent the equivalent computation using only real numbers (cf. Table I). The function $f_{1\mathbb{R}}$ is an equivalent computation to f_1 using only real-valued numbers and twice as many inputs and outputs to accommodate the real and imaginary parts of the complex numbers separately. We need three neurons in the hidden layer to represent x_1^2 , x_2^2 and $(x_1 + x_2)$. In the output layer we can then square the resulting value of the third hidden neuron and combine it with the (negative) identity of the first and second hidden neuron to construct the real and imaginary part of the output, each as a single real-valued number.

As for the network size we chose the theoretically optimal architecture size for CKAN and regular KAN respectively and also experimented with half the size of the optimal KAN architecture for CKAN and vice versa double the optimal size of CKAN for regular KAN. The grid size is $G = 8$ per dimension for CKAN and $G = 8 \cdot 8 = 64$ for real-valued KAN respectively.

Function $\mathbb{C} \rightarrow \mathbb{C}$	Function $\mathbb{R}^2 \rightarrow \mathbb{R}^2$
$f_1(z) = z^2$	$f_{1\mathbb{R}}(x, y) = \begin{pmatrix} x^2 - y^2 \\ 2xy \end{pmatrix}$
$f_2(z) = \sin(z)$	$f_{2\mathbb{R}}(x, y) = \begin{pmatrix} \sin(x) \cosh(y) \\ \cos(x) \sinh(y) \end{pmatrix}$
$f_3(z_1, z_2) = z_1 z_2$	$f_{3\mathbb{R}}(x_1, y_1, x_2, y_2) = \begin{pmatrix} x_1 x_2 - y_1 y_2 \\ x_1 y_2 + x_2 y_1 \end{pmatrix}$
$f_4(z_1, z_2) = (z_1^2 + z_2^2)^2$	$f_{4\mathbb{R}}(x_1, y_1, x_2, y_2) = \begin{pmatrix} x_1^2 + x_2^2 - y_1^2 - y_2^2 \\ 2x_1 y_1 + 2x_2 y_2 \end{pmatrix}^2$

TABLE I

OVERVIEW OF THE DIFFERENT FORMULAE USED IN OUR FUNCTION FITTING EXPERIMENTS. LEFT COLUMN FOR THE COMPLEX-VALUED FUNCTIONS AND RIGHT COLUMN FOR THEIR RESPECTIVE REAL-VALUED EQUIVALENTS, WITH $z = x + iy$. VECTOR NOTATION REPRESENTS THE SINGLE FEATURES THAT ARE FED INTO THE NETWORK. NOTE, THE OUTER SQUARE IN $f_{4\mathbb{R}}$ IS CALCULATED AS A MULTIPLICATION IN \mathbb{C} .

A total of 5000 points were randomly sampled inside our grid for every function and models of different sizes were trained for 1000 epochs using 5-fold cross validation.

The results of training on toy datasets generated by simple complex-valued formulae (cf. Table I) can be seen in Table II. For z^2 and $(z_1^2 + z_2^2)^2$ our CKAN is by far the best performing model when compared to FastKAN and KAN with similar or even bigger numbers of parameters. For $z_1 \cdot z_2$ CKAN is slightly better than FastKAN while CKAN requires only half the number of parameters. For $\sin(z)$ our approach is slightly worse than FastKAN, however FastKAN requires a bigger network size and thus ≈ 16 times as many parameters to perform marginally better than CKAN. With CKAN we are also able to achieve on average lower standard deviations on the results of the 5-fold cross validation, emphasizing the stability of our proposed model.

B. Physical Equations

For the physically meaningful formulae we use the same experimental setup as in subsection V-A. However, due to the higher complexity of this problem, we chose to generate datasets with 100,000 samples instead to cover the input space more thoroughly. The first formula we used to generate a dataset originates from holography, where we have a reference beam with electric field strength E_R and an object beam E_0 . To reconstruct the holography image, a second reconstruction beam \hat{E}_R is used. The formula for the reconstructed hologram - which we want to learn - then states:

$$H = \widehat{E}_R \cdot |E_R + E_0|^2 \quad (15)$$

The second formula describes an alternating current electric circuit consisting of a resistor with resistance R_L and a capacitor with impedance $\frac{1}{i\omega C}$ both in parallel to each other connected to a resistor R_G and a coil with impedance $i\omega L$ in series. R_L and R_G are the resistances measured in ohm, C is the capacitance of the capacitor measured in farad, L is the inductance of the coil measured in henry and ω is the frequency of electricity. We want to calculate the

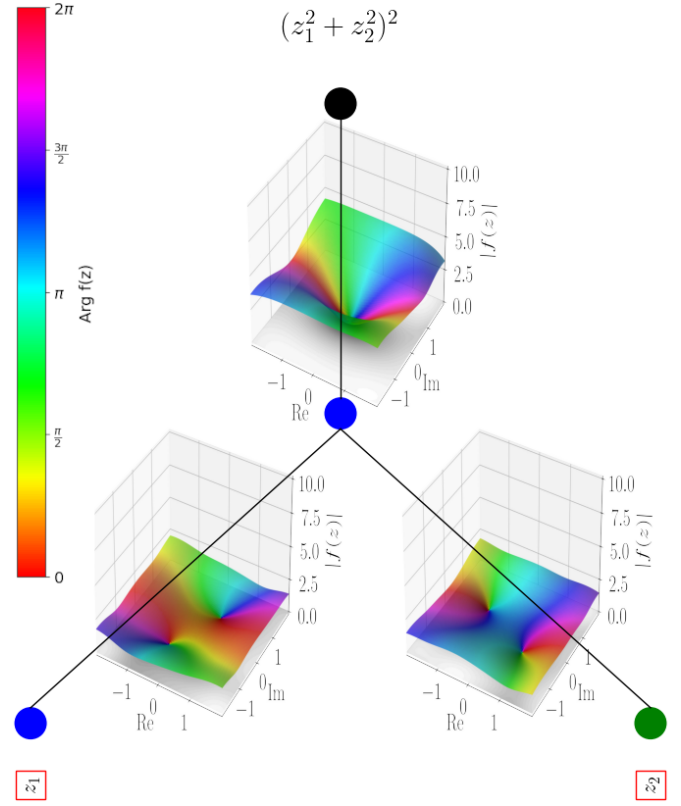


Fig. 3. Visualization of a CKAN for symbolic function fitting. Height of the graphs show magnitude of the learned function, colormap encodes the phase. Both functions on the lower edges represent quadratic functions with a constant offset. They sum to $z_1^2 + z_2^2$ since their offsets cancel out, which can be seen on the roots, which are identical besides a 90° rotation. The upper function represents a typical shape of a complex square function near the middle with some error artifacts on the edges of the grid.

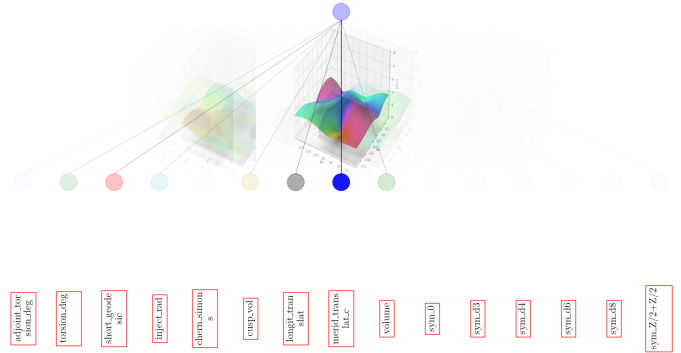


Fig. 4. Visualization of the first layer of a CKAN on the knot dataset with the opacity of edges and nodes proportional to their relevance score.

complex-valued voltage across the resistor \underline{U}_{R_L} when the other quantities are given:

$$\underline{U}_{R_L} = \frac{\underline{U}_G}{1 + \frac{R_G}{R_L} - \omega^2 \cdot L \cdot C + i\omega \cdot \left(\frac{L}{R_L} + R_G \cdot C\right)} \quad (16)$$

Note that the features R_G , R_L , L , C and ω are real-valued and only the two voltages \underline{U}_G and \underline{U}_{R_L} are complex-valued.

Dataset	Model	Size	# Params	Test MSE	Test MAE
z^2	CKAN	1×1	132	0.014 ±0.002	0.088 ±0.003
		1×2×1	538	0.013 ±0.004	0.097±0.016
	FastKAN	2×2	262	3.583 ±0.211	1.006±0.027
		2×3×2	791	0.195 ±0.068	0.305±0.061
	KAN	2×2	292	3.482 ±0.095	0.987±0.022
		2×3×2	876	0.260 ±0.097	0.316±0.078
$\sin(z)$	CKAN	1×1	132	0.005 ±0.001	0.051±0.002
		1×2×1	538	0.010 ±0.001	0.087±0.004
	FastKAN	2×2	262	0.478 ±0.029	0.506±0.016
		2×4×4×2	2106	0.004 ±0.001	0.047 ±0.007
	KAN	2×2	292	0.495 ±0.021	0.509±0.010
		2×4×4×2	2336	0.363 ±0.289	0.416±0.164
$z_1 * z_2$	CKAN	2×2×1	802	0.240 ±0.045	0.380±0.049
		2×4×2×1	2406	0.045 ±0.015	0.177 ±0.033
	FastKAN	4×4×2	1574	0.769 ±0.140	0.661±0.066
		4×8×4×2	4718	0.076 ±0.081	0.179±0.085
	KAN	4×4×2	1752	1.779 ±0.207	1.031±0.070
		4×8×4×2	5256	4.561 ±0.281	1.674±0.055
$(z_1^2 + z_2^2)^2$	CKAN	2×1×1	401	320.232 ±80.945	12.660±2.084
		2×4×2×1	2406	8.150 ±1.343	1.811 ±0.211
	FastKAN	4×2×2	788	364.340 ±30.439	13.180±0.598
		4×6×2×3×2	3155	442.129 ±54.164	13.688±0.707
	KAN	4×2×2	876	508.330 ±67.823	15.520±0.902
		4×6×2×3×2	3504	439.131 ±44.733	12.932±0.251

TABLE II
RESULTS OF CKAN, FASTKAN AND KAN ON FOUR DATASETS FOR FUNCTION FITTING.

However, the computation requires the use of complex-valued arithmetic.

The results of training on the holography dataset (cf. Table III) show that models with more parameters perform better. While our CKAN has the best MSE score, FastKAN performs better than our approach on MAE with less trainable parameters. This hints that the CKAN is more stable against outliers, but trades off this stability for a less accurate average result. When focusing on smaller - and thus more explainable - models, our model with size $3 \times 10 \times 1$ is the only small model to perform competitive with the best results.

A similar picture can be observed for the circuit dataset (cf. Table IV). In the MSE score, our CKAN outperforms other methods, however in the MAE score FastKAN performs better. Notably, on this dataset scaling up the model does not increase the performance meaningfully, with the best overall MAE score being obtained with the smallest FastKAN model.

C. Knot Classification

The knot dataset [37] originates from knot theory. Davies et al. calculated 15 invariants on $\approx 240,000$ different knots, from which 13 are real- and two complex-valued. Thus we need a real-valued KAN with 17 input features or a CKAN with 15 complex-valued input features, out of which 13 have their imaginary part set to zero. The task on this dataset is to classify the knots based on their invariants into 14 different classes representing their signature. Therefore the output layer’s width of both real- and complex-valued KANs is set to 14 to produce a probability vector. Since these probabilities are real-valued we need to learn a function $\mathbb{C} \rightarrow \mathbb{R}$ in the output layer as described in subsection IV-A. The features of the dataset are normalized to fit in our grid of fixed size $[-2, 2]$ for real-valued KANs and $[(-2 - 2i), (2 + 2i)]$ for CKAN.

Model	Size	# Params	Test MSE	Test MAE
CKAN	3×1	396	53.020 ±0.393	5.491±0.019
	3×1×1	533	41.889 ±0.222	4.861±0.017
	3×3×1	1599	6.598 ±0.234	2.038±0.035
	3×10×1	5330	0.151 ±0.006	0.310±0.011
	3×10×3×1	8381	0.168 ±0.043	0.300±0.037
	3×10×5×3×1	13026	0.112 ±0.029	0.240±0.028
FastKAN	6×1×2	525	27.986 ±0.587	3.687±0.057
	6×5×2	2617	7.640 ±2.454	1.903±0.306
	6×10×2	5232	2.869 ±0.491	1.182±0.108
	6×10×5×3×2	8571	0.140 ±0.102	0.227 ±0.077
KAN	6×1×2	584	38.295 ±6.309	4.141±0.282
	6×5×2	2920	15.890 ±0.508	2.745±0.035
	6×10×2	5840	1.853 ±1.096	0.801±0.341
	6×10×5×3×2	9563	45.596 ±4.760	4.757±0.215

TABLE III
RESULTS ON THE HOLOGRAPHY DATASET (15).

Model	Size	# Params	Test MSE	Test MAE
CKAN	6×1	792	7.166 ±1.343	1.008±0.010
	6×1×1	929	6.840 ±1.362	0.929±0.009
	6×3×1	2787	6.904 ±1.184	0.938±0.007
	6×10×1	9290	6.780 ±1.458	0.907±0.009
	6×10×3×1	12341	8.101 ±1.044	0.942±0.025
	6×10×5×3×1	16986	7.558 ±1.882	0.798±0.037
FastKAN	7×1×2	590	8.286 ±4.070	0.708 ±0.014
	7×5×2	2942	10.236 ±3.712	0.852±0.011
	7×10×2	5882	10.881 ±3.512	0.986±0.026
	7×10×5×3×2	9221	8.799 ±4.025	0.734±0.027
KAN	7×1×2	657	12.984 ±12.854	0.764±0.111
	7×5×2	3285	9.051 ±4.766	0.864±0.019
	7×10×2	6570	8.911 ±4.119	1.015±0.018
	7×10×5×3×2	10293	8.840 ±3.981	0.990±0.019

TABLE IV
RESULTS ON THE CIRCUIT DATASET (16).

Model	Size	#Params	Test Acc.	Test CE-Loss
CKAN	15×1×14	2921	0.923 ± 0.001	0.212 ± 0.001
	15×2×14	6754	0.944 ± 0.001	0.151 ± 0.003
FastKAN	17×1×14	296	0.739 ± 0.007	0.609 ± 0.005
	17×1×14	2032	0.893 ± 0.003	0.331 ± 0.013
	17×2×14	578	0.898 ± 0.002	0.259 ± 0.002
	17×2×14	4050	0.894 ± 0.016	0.315 ± 0.052
KAN	17×1×14	527	0.835 ± 0.009	0.442 ± 0.012
	17×1×14	2263	0.881 ± 0.007	0.620 ± 0.520
	17×2×14	1054	0.903 ± 0.033	0.282 ± 0.123
	17×2×14	4526	0.938 ± 0.001	0.184 ± 0.004

TABLE V

THE BEST-PERFORMING CKANS FOR HIDDEN LAYER WIDTHS $\in \{1, 2\}$, ALL EXPERIMENTS WITH FASTKAN AND KAN ON THE KNOT DATASET.

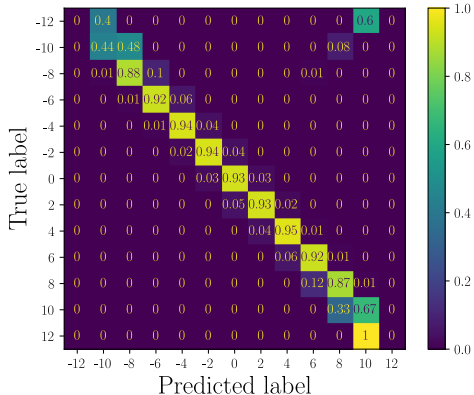


Fig. 5. Confusion matrix for CKAN on the knot dataset normalized to probabilities within each row.

In Table V we list the results of KAN, FastKAN, CKAN for hidden layer widths $\in \{1, 2\}$ and a grid size of $G = 8$. For the two real-valued KANs we also experimented with a grid size of $G = 64$ each to conduct a fairer comparison of our CKAN to the others. Our approach is the best-performing model on the knot dataset. While the best CKAN also has the highest number of parameters, the 15×1×14 CKAN performs still better than FastKAN and approximately equally well as KAN with a similar amount of parameters. In Fig. 5 an exemplary confusion matrix of our best performing CKAN is shown. The classes -12 and 12 are highly underrepresented in the dataset and thus CKAN does not learn anything for these classes. Besides these outliers, all classes are learned well.

Fig. 4 shows the first layer of a CKAN trained on the knot dataset with the opacity of nodes and edges showcasing the calculated relevance scores. Like in [1] the meridional, here as one single complex number, and longitudinal translation are the most relevant features. To also quantitatively evaluate the explainability, we conduct a small study, where we exclude less relevant features and retrain the model on only the more relevant features. When reducing the dataset with this method to 7 or 3 features, we still obtain good results, only reducing the accuracy by 0.012 and 0.028 respectively (cf. Table VI). In contrast, when we leave out these 7 or 3 most relevant features, the performance drops to $\approx 30\%$. This shows that this method determines the relevance of features accurately.

Features	# Params	Test Acc.	Test CE-Loss
all 15	2921	0.923 ± 0.001	0.212 ± 0.001
only 7 most important	1867	0.911 ± 0.003	0.233 ± 0.003
only 3 most important	1339	0.895 ± 0.002	0.267 ± 0.002
all but 7 most important	1999	0.284 ± 0.002	1.757 ± 0.003
all but 3 most important	2527	0.300 ± 0.003	1.663 ± 0.002

TABLE VI

RESULTS OF TRAINING A CKAN (WITH ONE INTERMEDIATE LAYER OF SIZE 1) ON THE FULL KNOT DATASET (15 FEATURES), AND USING ONLY THE MOST RELEVANT 7 OR 3 FEATURES OR LEAVING THESE OUT.

# Params	Normalization	CSiLU	Test Acc.	Test CE-Loss
2923	BN _C	c	0.921±0.001	0.213±0.001
		r	0.921±0.002	0.213±0.001
2921	BN _V	c	0.923 ±0.001	0.212 ±0.001
		r	0.921±0.001	0.213±0.001
2922	BN _{R2}	c	0.920±0.001	0.217±0.001
		r	0.920±0.001	0.213±0.001
2918	none	c	0.886±0.016	0.317±0.046
		r	0.789±0.153	0.591±0.445

TABLE VII

ABLATION STUDY ON THE INFLUENCE OF NORMALIZATION SCHEME AND CSiLU TYPE. EVALUATED ON A 15×1×14 CKAN ON THE KNOT DATASET.

D. Ablation Study

The ablation study regarding the influence of the used normalization scheme (cf. Section IV-C) and the choice of weights for CSiLU (cf. section IV-B) was conducted for the knot dataset and not for the synthetic function fitting datasets. We found in Table VII that normalization has a positive impact on the model but the choice of normalization scheme has little importance as BN_C, BN_V and BN_{R2} perform all similarly well but better than no normalization. As for the choice of CSiLU it shows that the complex-weighted variant CSiLU_C is always just as good or better than the real-weighted CSiLU_R.

VI. DISCUSSION

We have shown that CKAN has a clear advantage over the real-valued KANs when dealing with complex-valued function-fitting tasks. Our approach can compete with KAN and FastKAN while having less parameters and a shallower network architecture. These properties affect the explainability in a positive way. Furthermore our CKAN has proven to be more stable w.r.t. outliers in regression tasks since CKAN always produces one of the best MSE scores but is sometimes outperformed on the MAE metric. Our approach also produces more stable results across the five different runs of cross-validation for each configuration, which underlines the consistently good generalization capabilities of our model.

While CKAN does not excel on datasets with mostly real-valued features, like the circuit dataset in subsection V-B, it still performs similarly well as the real-valued KANs. If the datasets contain more complex numbers, CKAN can unfold it's full potential and outperform the real-valued KANs while requiring less parameters and having a shallower network structure, which improves the explainability.

Our tool for visualizing the proposed CKAN enables the understanding of the calculations happening inside our CKAN

and can thus help with (re-) discovering mathematical correlations in the data like Liu et al. pointed out in their real-valued KAN [1], [2]. The calculated importance scores reflect the true relevances of the features, as is shown by our experiments of training only on the 3 or 7 most important features or by leaving them out in Table VI. While the plot of our \mathbb{C} KAN trained on synthetic formula f_4 in Fig. 3 may seem unintuitive at first glance, the learned functions that are plotted show an interesting insight. In the bottom layer there exist two roots in both functions for z_1^2 and z_2^2 . The root points are exactly rotated around 90° when comparing those two functions. This is caused by shifts that cancel out:

$$(z_1^2 + s) + (z_2^2 - s) = z_1^2 + z_2^2 \quad (17)$$

Therefore we end up with roots at $\pm\sqrt{s}$ or $\pm\sqrt{-s}$ in the respective functions, which are identical roots up to $\sqrt{-1} = i$, which corresponds to a rotation of 90° in the complex plane.

Besides the qualitative visualization, the calculated relevance scores on the edges allow to analyze the importance of input as well as intermediate features. We show that this leads to meaningful results in our case study (cf. Table VI).

However, further research is required to study the actual explainability of KANs on real-world datasets.

VII. CONCLUSION

In this work we have developed \mathbb{C} KAN, a complex-valued variant of KAN, which relies on complex-valued RBFs. We have introduced BatchNorm to efficiently meet the problem of outputs exceeding the grid size of subsequent layers. In our experiment we could show that \mathbb{C} KAN outperforms the real-valued version KAN and FastKAN consistently on complex-valued tasks and performs on par or superior on tasks that mix complex- and real-valued inputs. Additionally, \mathbb{C} KAN training is more stable and leads to more explainable models, since less layers are needed to produce good results.

As future work, we aim to apply \mathbb{C} KAN to real world problems with complex-valued data, such as finding solutions to complex-valued PDEs by utilizing them in Kolmogorov-Arnold-Informed neural networks [4].

REFERENCES

- [1] Z. Liu, Y. Wang, S. Vaidya, F. Ruehle, J. Halverson, M. Soljačić, T. Y. Hou, and M. Tegmark, "KAN: Kolmogorov-Arnold Networks," *ICLR (accepted)*, 2025.
- [2] Z. Liu, P. Ma, Y. Wang, W. Matusik, and M. Tegmark, "KAN 2.0: Kolmogorov-Arnold networks meet science," *arXiv:2408.10205*, 2024.
- [3] R. Yu, W. Yu, and X. Wang, "KAN or MLP: A fairer comparison," *arXiv:2407.16674*, 2024.
- [4] Y. Wang, J. Sun, J. Bai, C. Anitescu, M. S. Eshaghi, X. Zhuang, T. Rabczuk, and Y. Liu, "Kolmogorov-Arnold-informed neural network: A physics-informed deep learning framework for solving forward and inverse problems based on Kolmogorov-Arnold networks," *Computer Methods in Applied Mechanics and Engineering*, vol. 433, p. 117518, 2025.
- [5] C. Lee, H. Hasegawa, and S. Gao, "Complex-valued neural networks: A comprehensive survey," *IEEE/CAA Journal of Automatica Sinica*, 2022.
- [6] J. Basseby, L. Qian, and X. Li, "A survey of complex-valued neural networks," *arXiv:2101.12249*, 2021.
- [7] Z. Li, "Kolmogorov-Arnold networks are radial basis function networks," *arXiv:2405.06721*, 2024.

- [8] J. Ahlberg, E. Nilson, and J. Walsh, "Complex cubic splines," *Transactions of the American Mathematical Society*, vol. 129, no. 3, pp. 391–413, 1967.
- [9] M. Unser and T. Blu, "Fractional splines and wavelets," *SIAM review*, vol. 42, no. 1, pp. 43–67, 2000.
- [10] B. Forster, T. Blu, and M. Unser, "Complex b-splines," *Applied and Computational Harmonic Analysis*, vol. 20, no. 2, pp. 261–282, 2006.
- [11] A. D. Bodner, A. S. Tepsich, J. N. Spolski, and S. Pourteau, "Convolutional Kolmogorov-Arnold networks," *arXiv:2406.13155*, 2024.
- [12] D. R. Cambrin, E. Poeta, E. Pastor, T. Cerquitelli, E. Baralis, and P. Garza, "KAN you see it? KANs and sentinel for effective and explainable crop field segmentation," *arXiv:2408.07040*, 2024.
- [13] M. Kiamari, M. Kiamari, and B. Krishnamachari, "GKAN: Graph Kolmogorov-Arnold networks," *arXiv:2406.06470*, 2024.
- [14] R. Bresson, G. Nikolentzos, G. Panagopoulos, M. Chatzianastasis, J. Pang, and M. Vazirgiannis, "KAGNNS: Kolmogorov-Arnold networks meet graph learning," *arXiv:2406.18380*, 2024.
- [15] X. Yang and X. Wang, "Kolmogorov-Arnold transformer," *arXiv:2409.10594*, 2024.
- [16] Y. Hou and D. Zhang, "A comprehensive survey on kolmogorov arnold networks (KAN)," *arXiv:2407.11075*, 2024.
- [17] W. Knottenbelt, Z. Gao, R. Wray, W. Z. Zhang, J. Liu, and M. Crispin-Ortuzar, "Coxkan: Kolmogorov-arnold networks for interpretable, high-performance survival analysis," *arXiv:2409.04290*, 2024.
- [18] E. Poeta, F. Giobergia, E. Pastor, T. Cerquitelli, and E. Baralis, "A benchmarking study of Kolmogorov-Arnold networks on tabular data," *arXiv:2406.14529*, 2024.
- [19] T. Alter, R. Lapid, and M. Sipper, "On the robustness of kolmogorov-arnold networks: An adversarial perspective," *arXiv:2408.13809*, 2024.
- [20] D. W. Abueidda, P. Pantidis, and M. E. Mobasher, "DeepOKAN: Deep operator network based on Kolmogorov Arnold networks for mechanics problems," *Computer Methods in Applied Mechanics and Engineering*, vol. 436, p. 117699, 2025.
- [21] A. Jamali, S. K. Roy, D. Hong, B. Lu, and P. Ghamisi, "How to learn more? Exploring Kolmogorov-Arnold networks for hyperspectral image classification," *Remote Sensing*, vol. 16, p. 4015, 2024.
- [22] A. Hirose, *Complex-Valued Neural Networks: Theories and Applications*. World Scientific, 2003.
- [23] C. Trabelsi, O. Bilaniuk, Y. Zhang, D. Serdyuk, S. Subramanian, J. F. Santos, S. Mehri, N. Rostamzadeh, Y. Bengio, and C. J. Pal, "Deep complex networks," in *International Conference on Learning Representations*, 2018.
- [24] Z.-H. Tan, Y. Xie, Y. Jiang, and Z.-H. Zhou, "Real-valued backpropagation is unsuitable for complex-valued neural networks," *Advances in Neural Information Processing Systems*, vol. 35, pp. 34052–34063, 2022.
- [25] F. Eilers and X. Jiang, "Building blocks for a complex-valued transformer architecture," in *IEEE International Conference on Acoustics, Speech and Signal Processing (ICASSP)*, 2023.
- [26] H. Zhang, M. Gu, X. Jiang, J. Thompson, H. Cai, S. Paesani, R. Santagati, A. Laing, Y. Zhang, M. Yung, *et al.*, "An optical neural chip for implementing complex-valued neural network," *Nature Communications*, vol. 12, no. 1, p. 457, 2021.
- [27] C. Zhong, X. Sang, B. Yan, H. Li, D. Chen, X. Qin, S. Chen, and X. Ye, "Real-time high-quality computer-generated hologram using complex-valued convolutional neural network," *IEEE Transactions on Visualization and Computer Graphics*, 2023.
- [28] H. Chen, F. He, S. Lei, and D. Tao, "Spectral complexity-scaled generalisation bound of complex-valued neural networks," *Artificial Intelligence*, vol. 322, p. 103951, 2023.
- [29] X. Liu, J. Yu, T. Kurihara, C. Wu, Z. Niu, and S. Zhan, "Pixelwise complex-valued neural network based on 1d FFT of hyperspectral data to improve green pepper segmentation in agriculture," *Applied Sciences*, vol. 13, no. 4, p. 2697, 2023.
- [30] P. Xing, J. Porée, B. Rauby, A. Malescot, E. Martineau, V. Perrot, R. L. Rungta, and J. Provost, "Phase aberration correction for in vivo ultrasound localization microscopy using a spatiotemporal complex-valued neural network," *IEEE Transactions on Medical Imaging*, 2023.
- [31] A. Yakupoğlu and Ö. C. Bilgin, "Comparison of complex-valued and real-valued neural networks for protein sequence classification," *Neural Computing and Applications*, pp. 1–14, 2024.
- [32] S. Chen, X. Hong, C. J. Harris, and L. Hanzo, "Fully complex-valued radial basis function networks: Orthogonal least squares regression and

- classification,” *Neurocomputing*, vol. 71, no. 16-18, pp. 3421–3433, 2008.
- [33] J. A. Soares, V. H. Luiz, D. S. Arantes, and K. S. Mayer, “Deep complex-valued radial basis function neural networks and parameter selection,” in *19th International Symposium on Wireless Communication Systems (ISWCS)*, 2024, pp. 1–6.
- [34] A. N. Kolmogorov, “On the representation of continuous functions of many variables by superposition of continuous functions of one variable and addition,” *Dokl. Akad. Nauk SSSR*, no. 5, pp. 953–956, 1957.
- [35] F. Girosi and T. Poggio, “Representation properties of networks: Kolmogorov’s theorem is irrelevant,” *Neural Computation*, vol. 1, no. 4, pp. 465–469, 1989.
- [36] S. Ioffe, “Batch normalization: Accelerating deep network training by reducing internal covariate shift,” *arXiv:1502.03167*, 2015.
- [37] A. Davies, P. Veličković, L. Buesing, S. Blackwell, D. Zheng, N. Tomašev, R. Tanburn, P. Battaglia, C. Blundell, A. Juhász *et al.*, “Advancing mathematics by guiding human intuition with AI,” *Nature*, vol. 600, no. 7887, pp. 70–74, 2021.